© 2018. Published by The Company of Biologists Ltd | Development (2018) 145, dev157909. doi:10.1242/dev.157909

RESEARCH ARTICLE

ELMO and Sponge specify subapical restriction of Canoe and formation of the subapical domain in early *Drosophila* embryos

Anja Schmidt*, Zhiyi Lv* and Jörg Großhans‡

ABSTRACT

Canoe/Afadin and the GTPase Rap1 specify the subapical domain during cellularization in *Drosophila* embryos. The timing of domain formation is unclear. The subapical domain might gradually mature or emerge synchronously with the basal and lateral domains. The potential mechanism for activation of Rap1 by guanyl nucleotide exchange factors (GEFs) or GTPase activating proteins (GAPs) is unknown. Here, we retraced the emergence of the subapical domain at the onset of cellularization by *in vivo* imaging with CanoeYFP in comparison to the lateral and basal markers ScribbledGFP and CherrySlam. CanoeYFP accumulates at a subapical position at about the same time as the lateral marker ScribbledGFP but a few minutes prior to basal CherrySlam. Furthermore, we show that the unconventional GEF complex ELMO-Sponge is subapically enriched and is required for subapical restriction of Canoe. The localization dynamics of ELMO-Sponge suggests a patterning mechanism for positioning the subapical region adjacent to the apical region. While marking the disc-like apical regions before cellularization, ELMO-Sponge redistributes to a ring-like pattern surrounding the apical region at the onset of cellularization.

KEY WORDS: *Drosophila*, Cortical domains, Epithelial domains, Epithelial polarity, Subapical, F-actin, Small GTPase, Guanyl nucleotide exchange factor, Cellularization, Ced-12

INTRODUCTION

Cortical domains (apical, subapical, lateral, basal) are a characteristic feature of epithelial cells and are crucial for their diverse functions (Hermiston and Gordon, 1995; Martín-Belmonte et al., 2008; Stephenson et al., 2010). Cortical domains are defined by integral membrane proteins, such as Crumbs and E-Cadherin, as well as membrane-associated proteins such as the Par proteins (Chalmers et al., 2005; Cohen et al., 2004; Izumi et al., 1998), in addition to lipid composition (reviewed by Gassama-Diagne and Payrastre, 2009). In many cases, the separation of the domains is maintained by mutual exclusion of determinants, such as the lateral exclusion of Bazooka (Baz; also known as Par-3) by Par-1 and Scribbled (Scrib or Scrb) (Benton and Johnston, 2003; Bilder et al., 2003). By contrast, the mechanisms for initial establishment and arrangement of cortical regions are less clear.

During embryonic development of *Drosophila*, epithelial cells emerge at the cellular blastoderm stage in a process called cellularization. Following a stage of syncytial development that includes 13 nuclear cycles, ∼6000 cortical nuclei are synchronously enclosed into individual cells in interphase 14 as the plasma membrane invaginates between adjacent nuclei (reviewed by Foe et al., 1993). Cellularization leads to a monolayered columnar epithelium with four distinct cortical regions and adherens junctions positioned at the subapical region. Prior to cellularization, only two cortical regions can be differentiated, namely the cap and intercap regions in syncytial embryos (Warn et al., 1980, 1984). During mitosis of the nuclear cycles, the spindles are separated by a metaphase furrow up to 10 µm deep (Sherlekar and Rikhy, 2017). Three cortical regions are found within the metaphase furrow: the apical, lateral and basal regions (Mavrakis et al., 2009). The change of cellular organization and switch from syncytial to cellular development is a central feature of the mid-blastula transition (MBT), in addition to cell cycle remodeling, degradation of maternal RNA and activation of zygotic transcription (reviewed by Farrell and O'Farrell, 2014; Liu and Großhans, 2017; Yuan et al., 2016).

Here, we focus on the subapical region, which, in contrast to the other cortical regions, emerges during cellularization. It has been suggested that the subapical region matures gradually, since Baz, the typical subapical determinant, and the E-Cadherin (Shotgun) complex gradually accumulate during the course of cellularization and are properly positioned only by the end of cellularization (Harris and Peifer, 2004; McGill et al., 2009). Subapical restriction of Baz and E-Cadherin depends on the actin-binding protein Canoe (Cno)/Afadin and its regulator, the Rap1 GTPase (Choi et al., 2013; Sawyer et al., 2009). Histological analysis of fixed embryos suggested that Canoe marks the subapical domain prior to Baz (Choi et al., 2013). The timing of initial subapical accumulation of Canoe has not been retraced. As a GTPase, Rap1 is potentially regulated by an upstream guanyl nucleotide exchange factor (GEF) or a GTPase activating protein (GAP). The unconventional GEF complex ELMO (Ced-12)-Sponge (Spg)/DOCK represents a candidate (Geisbrecht et al., 2008; Postner et al., 1992; Winkler et al., 2015). Biochemical analysis indicates that ELMO-DOCK complexes are GEF-specific for Rac and Rap1 (Biersmith et al., 2011, 2015; deBakker et al., 2004; Yajnik et al., 2003; Wu and Horvitz, 1998). Although a role of *sponge* in the organization of actin caps in syncytial embryos was reported some time ago (Postner et al., 1992), a function in the context of the subapical domain or of Canoe has not been investigated.

In this study, we show by live imaging that the cortical markers Canoe, Scribbled and Slam segregate during the first minutes of cellularization. Analyzing the mutant phenotypes of *ELMO* (*Ced-12*) and *sponge*, we identify them as an upstream factor in Canoe localization. We report the dynamics of Sponge and ELMO protein in fixed and live embryos. Sponge and ELMO mark the apical regions, which are characterized by strong F-actin staining ('actin caps') of the plasma membrane during the syncytial blastoderm stage prior to cellularization. Strikingly, this localization pattern

Institute for Developmental Biochemistry, University of Göttingen, Justus-von-Liebig Weg 11, 37077 Göttingen, Germany.
*These authors contributed equally to this work

‡Author for correspondence (joerg.grosshans@med.uni-goettingen.de)

J.G., 0000-0003-1114-9233

Received 30 July 2017; Accepted 18 December 2017

Development (2018) 145, dev157909. doi:10.1242/dev.157909

changes at the onset of cellularization. ELMO and Sponge redistribute to the rims of the actin caps and surround the apical regions and thus generate the information for a new region. Essentially, the distribution changes from a disc-like to a ring-like pattern. Based on this dynamic, we propose a model for pattern formation in which the subapical domain is positioned adjacent to the apical domain.

RESULTS

Emergence of the subapical domain during the onset of cellularization

Stereotypic and stage-specific changes in cortical organization are linked to early embryonic development (Nance, 2014). In *Drosophila*, a uniformly structured cortex is characteristic for the preblastoderm stage (Karr and Alberts, 1986). When the first nuclei reach the cortex in nuclear cycle 9, their associated centrosomes induce cortical differentiation and segregation of cortical markers into disc-like caps or cytoplasmic buds, rich in F-actin, and the region between the caps (intercap), which is marked by Slam and Toll (Fig. 1A) (Mavrakis et al., 2009; Raff and Glover, 1989; Warn et al., 1984). The cortex is further differentiated during syncytial mitoses. By immunostaining, we detected three cortical domains: Slam at the furrow tip, Discs large (Dlg, or Dlg1) at the furrow, and Canoe apically and at the furrow (Fig. 1B).

An important feature of MBT and the transition from syncytial to cellular development is the emergence of a subapical domain and of a typical epithelial cortex with four domains. The subapical domain is inserted between the apical and lateral domains. Canoe is the most upstream acting subapical marker (Choi et al., 2013). During syncytial mitoses. We detected Canoe at the apical and lateral regions. Staining was excluded from the basal domain (Fig. 1C). The cortical distribution profoundly changes in interphase 14, when Canoe became restricted to the subapical domain and segregated from the lateral marker Dlg (Fig. 1D,E). In contrast to Canoe, other subapical markers such as Baz, Par-6, aPKC and E-Cadherin accumulate gradually at the subapical region during the course of cellularization (Harris and Peifer, 2004; McGill et al., 2009; Wang et al., 2004).

To achieve a precise timing and reveal the dynamics of subapical accumulation of Canoe, we conducted time-lapse imaging of embryos expressing CanoeYFP from its endogenous locus in comparison with the lateral marker ScribbledGFP or the basal marker CherrySlam (Fig. 2, Figs S1 and S2). As we reported previously (Acharya et al., 2014), Slam continuously marks the transition from the retracting metaphase furrows to cellularization furrows (‘old’ furrow). Within a few minutes, Slam accumulates at the ‘new’ furrow. For comparative timing, we refer to the formation of the furrow between corresponding daughter nuclei and to the retraction of the metaphase furrow. During telophase, the retracting metaphase furrow (old furrow) encloses corresponding daughter nuclei, while a shallow groove (new furrow) emerges between them (Fig. 2A).

We found that CanoeYFP (Fig. 2A,B, t=3 min) and ScribbledGFP (Fig. 2A,C, t=1 min) were uniformly dispersed following retraction of the metaphase furrow. Within a few minutes, however, a restriction of both markers became apparent at the prospective furrow (Fig. 2B,C, t=7 min). CherrySlam accumulated slightly later than CanoeYFP at the new furrow. A clear signal was observed starting at t=8-12 min (Fig. 2B,D,E). This difference between CanoeYFP and CherrySlam was also observed along the apical-basal axis. CanoeYFP reached high levels at a position between 2 and 3 µm (Fig. 2D,E). CherrySlam showed the strongest signal a few minutes later at a position of ∼4 µm (Fig. 2D,E). The appearance of CherrySlam in the basal layer is probably linked to the invagination of the new furrow. These data describe a clear segregation of the subapical and basal markers already at t=8 min. This represents the earliest time that the two markers are clearly separated. We also observed a difference in the accumulation of the lateral marker ScribbledGFP. We detected a strong signal at position 3-5 µm (Fig. 2F), which was more basal than the peak of CanoeYFP. Domain restriction and furrow formation also became obvious when considering the width of the new furrow (Fig. 2G, Fig. S3). Within 10 min, the width of the CanoeYFP region was gradually reduced from 2.5 µm to 0.5 µm. In summary, our live imaging analysis shows that the cortical domains form within ∼10 min after exit from mitosis 13. Analyses of both fixed and live embryos show that Canoe marks the subapical domain throughout cellularization, suggesting that the subapical domain forms together with the basal and lateral domains and does not gradually arise during cellularization.

Staining and live analysis revealed a mutually exclusive distribution of Canoe, Scribbled and Slam. We examined whether this pattern depended on the function of these proteins. We first

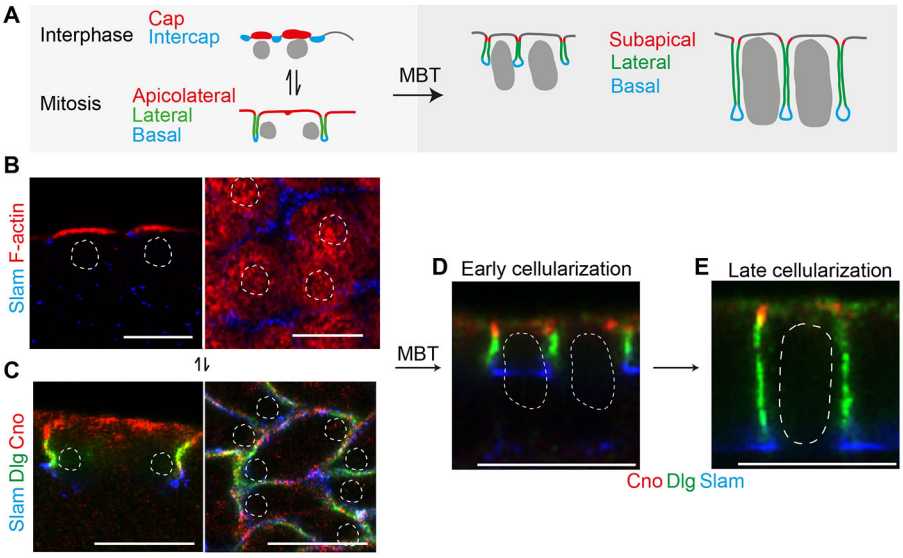

Fig. 1. Dynamics in cortical domains in the *Drosophila* blastoderm embryo. (A) Scheme (sagittal view) illustrating cortical domains (color coded) before and after mid-blastula transition (MBT). (B-E) Embryos stained for domain markers before and after MBT. (B) Interphase 13, stained for caps (F-actin) and intercap regions (Slam) in sagittal and planar view. (C) Mitosis 12, stained for the apical-lateral (Canoe), lateral (Dlg) and basal (Slam) domains. Early (D) and late (E) cellularization (interphase 14), sagittal view, stained for subapical (Canoe), lateral (Dlg) and basal (Slam) domains. Dashed lines outline nuclei. Scale bars: 10 µm.

Development (2018) 145, dev157909. doi:10.1242/dev.157909

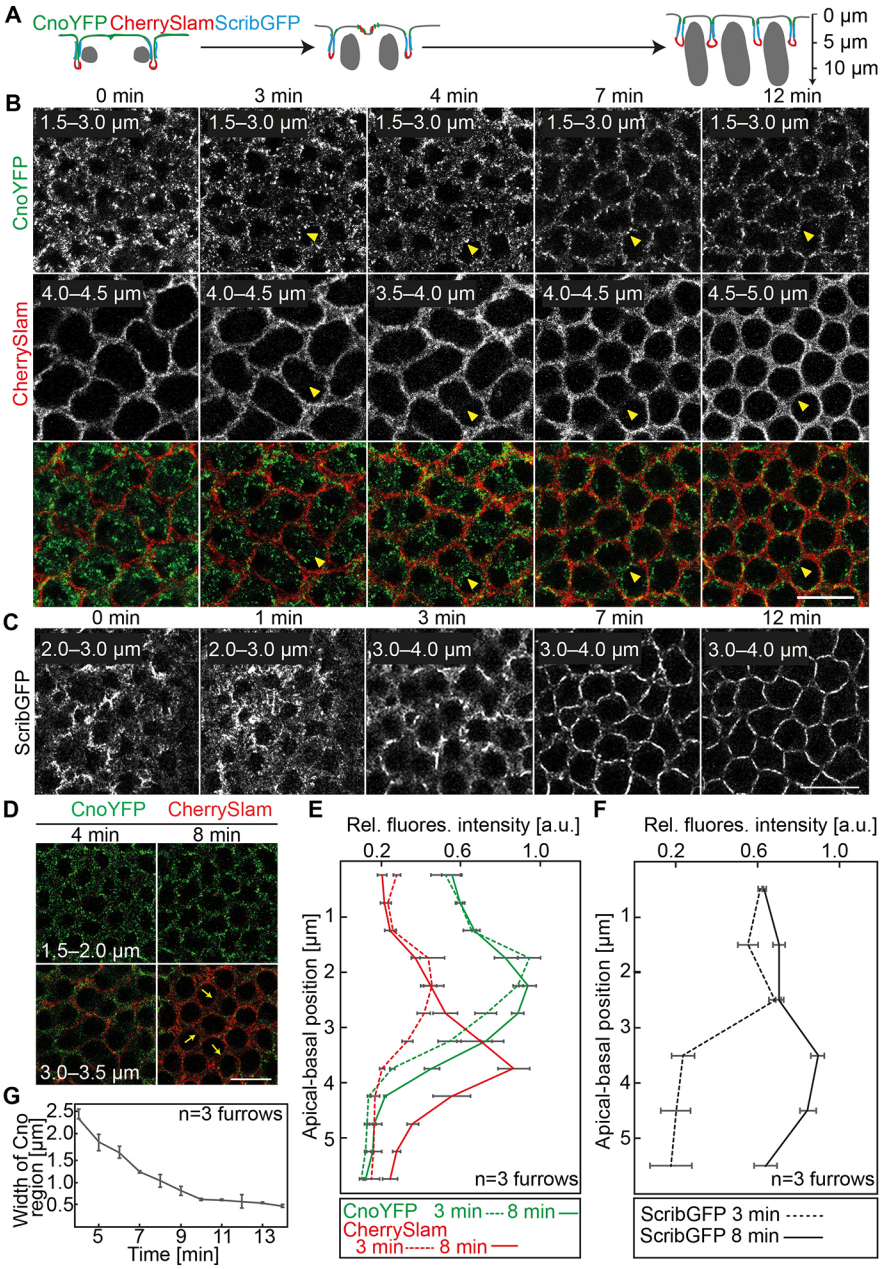

Fig. 2. Dynamics of Canoe, Scribbled and Slam during cellularization. (A) Scheme for furrow formation and invagination in early cellularization. CanoeYFP, CherrySlam and ScribbledGFP mark subapical, basal and lateral domains, respectively (color coded). Axial (apical-basal) axis with approximate scale is indicated on the right. (B-D) Images from time-lapse recordings including axial stacks of embryo expressing (B,D) CanoeYFP (gray/green) and CherrySlam (gray/red) or (C) ScribbledGFP during mitosis 13 and early interphase 14. Axial position is indicated. Yellow arrowheads and arrows point to the position of 'new' furrows. (E,F) Relative fluorescence intensity of (E) CanoeYFP, CherrySlam and (F) ScribbledGFP at new furrows measured along the apical-basal axis at the indicated times. (G) Width of CanoeYFP fluorescence signal across new furrows plotted against time. Error bars represent s.e.m. Scale bars: 10 µm.

confirmed previous reports that membrane association of Canoe depends on Rap1 (Choi et al., 2013) (Fig. 3A,B). By contrast, subapical Canoe restriction depended neither on *slam* (Fig. 3E) nor *scribbled* (Fig. 3D). We stained embryos from *scribbled* or *slam* germline clones (hereafter referred to as *scribbled* and *slam* mutants) for Canoe and the lateral marker Dlg. In *scribbled* mutants, we detected subapically restricted Canoe (Fig. 3D). Consistent with previous reports on the mutual dependency of Scribbled and Dlg (Bilder et al., 2003), Dlg was spread over and loosely associated with the membrane in *scribbled* mutants. Similarly, Canoe was subapically restricted in *slam* mutants (Fig. 3E). Although furrow invagination is impaired, furrows are specified in *slam* mutants (Acharya et al., 2014). These data show that the initial accumulation of the subapical marker Canoe does not depend on *scribbled* and *slam*, and that independent pathways at the level of *canoe*, *scribbled* and *slam* might define the respective cortical domains.

The unconventional GEF complex ELMO-Sponge controls subapical Canoe restriction

The GTPase Rap1 is presumably controlled by GEFs or GAPs, such as the GEF protein Dizzy (Dzy; also known as PDZ-GEF) (Huelsmann et al., 2006; Spahn et al., 2012) or the heteromeric GEF complex ELMO-Sponge (Fig. 4E) (Biersmith et al., 2011; Yajnik et al., 2003). To test this hypothesis, we analyzed *dizzy* mutant embryos for subapical restriction of Canoe. In embryos from *dizzy* germline clones, we did not detect a deviation of Canoe staining as compared with wild-type embryos (Fig. 3C). By contrast, Canoe was spread along the cellularization furrow in embryos from *ELMO* germline clones (Fig. 5B,D) and embryos from *sponge* mutant females (Fig. 5C); these embryos are hereafter designated as *ELMO* and *sponge* embryos. *ELMO* embryos passed through a normal number of nuclear divisions, but failed to form actin caps and metaphase furrows during syncytial cycles (Fig. 4B) (Winkler et al., 2015). Associated with this morphological

Development (2018) 145, dev157909. doi:10.1242/dev.157909

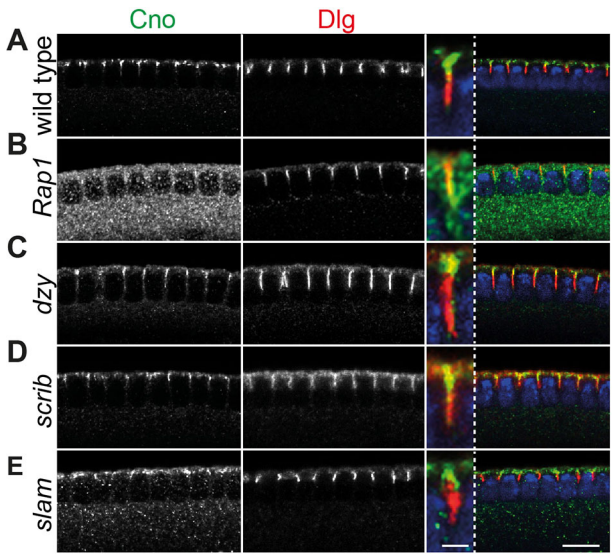

Fig. 3. Genetic control of subapical Canoe. Fixed embryos in early cellularization stained for Canoe (gray/green), Dlg (gray/red) and DNA (blue). Merged images are on the right, with insets showing high magnification of one furrow. Genotypes: (A) wild type; embryos from germline clones for (B) *Rap1*, (C) *dizzy*, (D) *scribbled*, (E) *slam*. Scale bars: 10 µm; insets, 2 µm.

phenotype were chromosomal segregation defects and subsequent fallout of nuclei. In interphase 14, they cellularized at the anterior and posterior termini but not in the medial region (Fig. 4C). We observed a similar phenotype in *sponge* embryos, which is consistent with a previous report (Postner et al., 1992).

Canoe spread along the cellularization furrows in *ELMO* and *sponge* embryos, whereas the lateral marker Dlg and the basal marker Slam localized normally (Fig. 5B,C). We quantified the distribution of Canoe along the cellularization furrow by plotting the relative fluorescence along the apical-basal axis. We did not compare absolute protein levels. Whereas restriction to the subapical domain was observed in wild-type embryos (Fig. 5A, D), Canoe was spread all along the furrow in *ELMO* embryos (Fig. 5B,D). These data show that *ELMO* and *sponge* are required for subapical restriction of Canoe.

Subapical restriction of ELMO and Sponge during cellularization

Functioning upstream of Canoe, the ELMO-Sponge complex might confer positional information for the subapical domain, in that ELMO or Sponge would localize to the prospective subapical region no later than when subapical restriction of Canoe is observed. To test this hypothesis, we analyzed the dynamics and localization pattern of ELMO and Sponge. Since a suitable antibody was available (Biersmith et al., 2011), we fixed and stained wild-type embryos for Sponge (Fig. 6). We detected Sponge at the caps in syncytial cycles. During syncytial mitoses, uniform Sponge staining was detected at the apical and lateral membranes. A strikingly different pattern was observed in embryos during cellularization. We detected a staining pattern clearly restricted to the subapical domain and largely separated from the lateral marker Dlg throughout cellularization (interphase 14). The subapical restriction of Sponge was not as clear as that observed for Canoe, however. Importantly, Sponge staining was depleted in the apical region, leading to a grid-like pattern in the surface view, even when the apicalmost layers were included in the projections (Fig. 6).

The subapical staining pattern of Sponge did not depend on *scribbled*, *canoe* or *Rap1*. We detected subapical restriction of Sponge in *scribbled*, *Rap1* and *canoe* germline clones (hereafter *scribbled*, *Rap1* and *canoe* mutants) (Fig. 7A-D). These data indicate that Sponge functions independently and possibly upstream of the Rap1-Canoe pathway. In contrast to *Rap1*, *canoe* and *scribbled*, the subapical localization of Sponge depends on ELMO. When we stained *ELMO* mutants for Sponge, the Sponge signal was uniformly distributed and no membrane association was detected (Fig. 7E). The loss of membrane association and restricted localization are consistent with the structure of the ELMO-Sponge complex, in which ELMO provides membrane binding and Sponge the GEF activity (Fig. 4E) (Komander et al., 2008).

To record the dynamics of the ELMO-Sponge complex at high temporal resolution, we generated an ELMO-GFP fusion protein expressed from a genomic transgene (Fig. 4A). The ELMO-GFP fusion protein was expressed at comparable levels as from the wild-type allele (Fig. 4D) and was functional, as it rescued the germline clone phenotype of *ELMO*. During syncytial cycles, we detected ELMO-GFP at the caps (Fig. 8A). With the onset of cellularization,

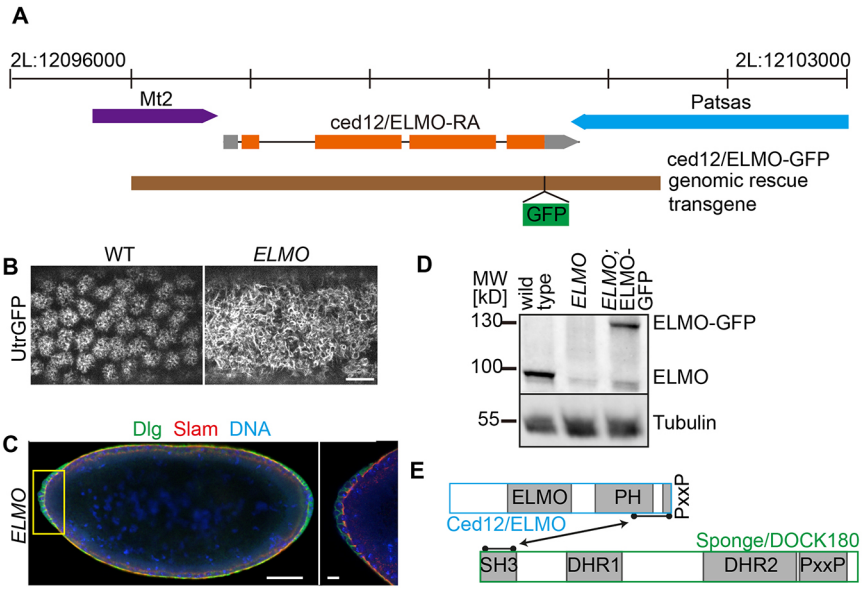

Fig. 4. Blastoderm phenotype of embryos from *ELMO* germline clones. (A) *ELMO* locus on chromosome 2L. Genomic rescue construct ELMO-GFP is indicated by the brown bar. (B) Wild-type and *ELMO* embryos expressing the F-actin marker UtrGFP. (C) Fixed *ELMO* embryo stained for Dlg, Slam and DNA. The cellularizing terminus marked by the yellow rectangle is magnified in the inset. (D) Embryonic extracts from wild-type, *ELMO*, and *ELMO* embryos with the genomic ELMO-GFP rescue transgene were analyzed by western blot with ELMO and α-Tubulin (loading control) antibodies. (E) Domain structures of ELMO and Sponge. Interaction domains are marked by double-headed arrow. Scale bars: 50 µm in C; 10 µm in B and in inset in C.

Development (2018) 145, dev157909. doi:10.1242/dev.157909

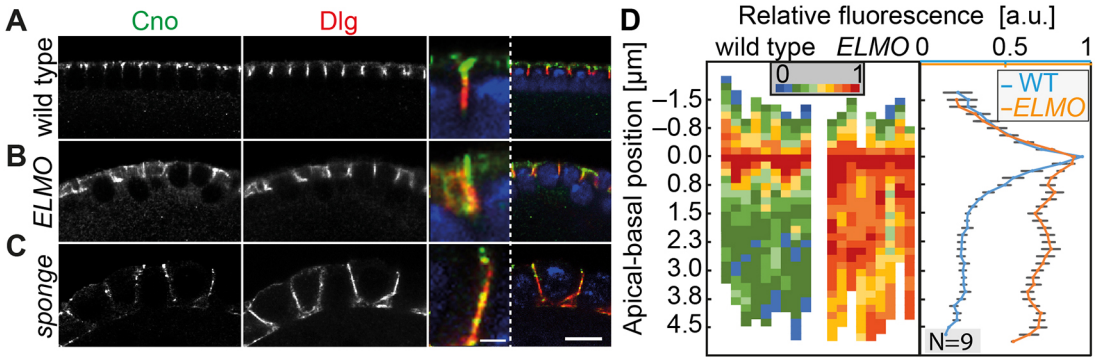

Fig. 5. *ELMO* and *sponge* are required for subapical restriction of Canoe. (A-C) Fixed wild-type (A), *ELMO* (B) and *sponge* (C) embryos stained for Canoe (gray/green), Dlg (gray/red) and DNA (blue). Insets show higher magnification of one furrow from merge. (D) Heatmaps and averaged values of relative fluorescence intensity along the apical-basal axis for multiple furrows aligned to the peak value (nine furrow in three embryos). Error bars represent s.e.m. Scale bars: 10 µm; insets, 2 µm.

the localization pattern of ELMO-GFP changed profoundly from the disc-like pattern in syncytial interphases to a ring-like pattern (Fig. 8B, C, arrowheads; Fig. S4). ELMO-GFP signal at new furrows was first detected at about the time when CanoeYFP accumulates at the apical region (Fig. 2). We quantified the relative fluorescence intensity along the apical-basal axis of new furrows and compared the profile to CherrySlam fluorescence (Fig. 8D). We observed an early subapical accumulation and subsequent restriction of ELMO-GFP, whereas CherrySlam accumulated a few minutes later at a basal position.

DISCUSSION

In this study, we have focused on analysis of the functional relationships of cortical domains and their associated proteins in terms of the insertion of a new domain at a specific time and place. Based on *in vivo* and *in vitro* studies of ELMO-Sponge/DOCK, Rap1 and Canoe/Afadin in other experimental systems, we have some understanding of their biochemical activities (Biersmith et al., 2011; Boettner et al., 2003; Sawyer et al., 2009). In biochemical assays, the ELMO-Sponge complex specifically activates Rac and Rap1 among the small GTPases (Yajnik et al., 2003). ELMO-Sponge might activate Rap1 in the subapical region during the onset of cellularization (Fig. 9). As a consequence, activated Rap1-GTP may restrict Canoe to the subapical domain. We analyzed the distribution of Rap1 employing Rap1-GFP as a proxy. As we detected a wide and uniform distribution of Rap1-GFP over the plasma membrane (Fig. S5), Rap1 distribution cannot be used as a test for whether ELMO-Sponge would activate Rap1. Alternatively, ELMO-Sponge might act on Canoe independently of Rap1 (Fig. 9), as we have not demonstrated that Rap1 links ELMO-Sponge and Canoe or that Rap1 is activated by ELMO-Sponge.

During the course of cellularization, Canoe will gradually recruit the polarity protein Baz (Par-3) and subsequently the E-Cadherin complex to this domain in order to make it into a generic subapical domain. When comparing their distributions, Canoe is more clearly localized than ELMO-Sponge. This difference might be due to the signaling process. In the simple model, the pathway initiated by

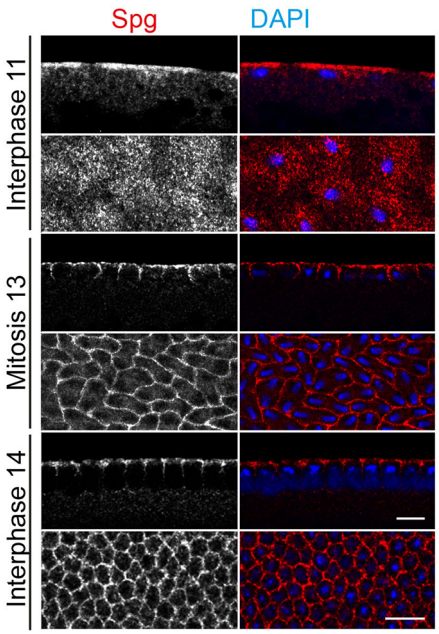

Fig. 6. Subapical restriction of Sponge. Fixed wild-type embryos at indicated stages stained for Sponge (gray/red) and DNA (blue). Sagittal and planar views. Scale bars: 10 µm.

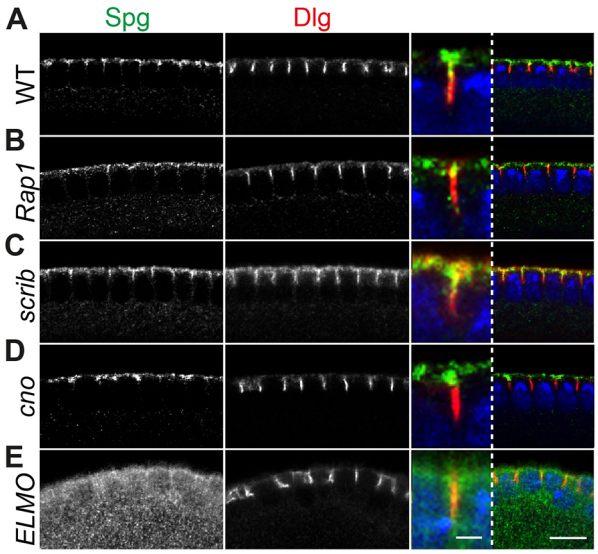

Fig. 7. Genetic control of subapical Sponge. Fixed embryos in early cellularization stained for Sponge (gray/green), Dlg (gray/red) and DNA (blue). Insets show higher magnification of one furrow from merge. Genotypes: (A) wild type; embryos from germline clones for (B) *Rap1*, (C) *scribbled*, (D) *canoe*, (E) *ELMO*. Scale bars: 10 µm; insets, 2 µm.

Development (2018) 145, dev157909. doi:10.1242/dev.157909

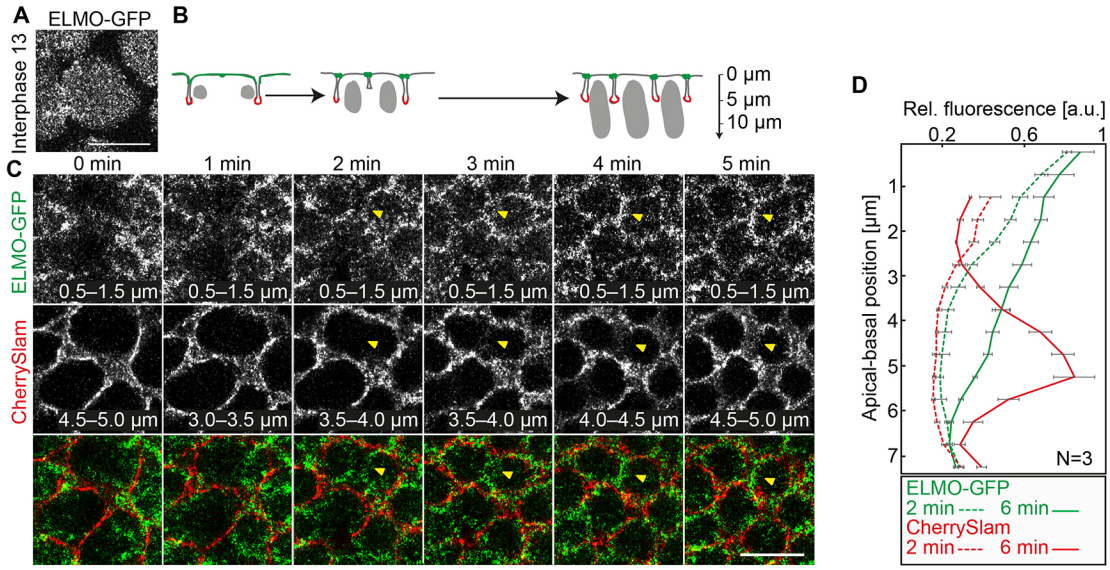

Fig. 8. Dynamics of ELMO-GFP during early cellularization. (A) Image from a time-lapse recording of an embryo expressing ELMO-GFP shows ELMO-GFP localization at the cap during interphase 13. (B) Scheme for furrow formation and invagination in early cellularization. Subapical and basal domains are marked in green and red, respectively. Axial (apical-basal) axis with approximate scale is indicated. (C) Images from time-lapse recordings including axial stacks of embryo expressing ELMO-GFP (gray/green) and CherrySlam (gray/red) during mitosis 13 and early interphase 14. Axial position is indicated. Yellow arrowheads point to position of new furrows. (D) Relative fluorescence intensity of ELMO-GFP and CherrySlam at new furrows measured along the apical-basal axis at the indicated times (three furrows). Error bars represent s.e.m. Scale bars: 10 µm.

ELMO-Sponge via Rap1 and Canoe is linear. We do not rule out reinforcing feed-back interactions within the pathway that lead to enhanced signals. Such feedback interactions are likely to be important for maintenance of the subapical domain. For example, Baz influences Canoe localization later in cellularization (Choi et al., 2013). In the accompanying paper, Bonello et al. (2018) describe a function of *dizzy* in the apical restriction and especially localization of Canoe to tricellular junctions via activation of Rap1 during late cellularization.

When studying the initial formation of the subapical domain, we have not observed an influence of the lateral determinant Scribbled or the basal protein Slam. Such interactions are likely to be important later in cellularization and development for maintenance of the cortical domains or sharpening of the boundaries, as it is well established that lateral and subapical components interact by mutual exclusion (Bilder et al., 2003; Tanentzapf and Tepass, 2003).

The change in ELMO-Sponge distribution from a disc-like pattern during the nuclear cycles to a ring-like pattern during initial cellularization suggests a model for the origin of positional information for the emerging subapical domain (Fig. 9A). The organization in cap and intercap regions already contains the information for a third domain, namely the interface between the two regions (Fig. 9B). The dynamic localization pattern of ELMO-Sponge makes use of this information in initial cellularization. Whereas uniformly distributed within the caps during syncytial cycles, ELMO-Sponge accumulates at the rims of the apical region during the onset of cellularization. Subsequently, when the furrows invaginate, adjacent rings around the apical regions meet to form a grid-like pattern.

The determinants for specific membrane localization of ELMO-Sponge are not clear. Within the ELMO-Sponge complex (Fig. 4E), membrane association is assumed to be conferred by ELMO. The role of the conserved ELMO domain is unclear (Komander et al., 2008). The PH domain might mediate membrane association by binding phospholipids. However, no corresponding subapical localization pattern of phospholipids has been reported. Sensor proteins for $PI(4,5)P_2$ and $PI(3,4,5)P_3$ were reported to be widely distributed along the invaginating furrow (Reversi et al., 2014). As an alternative to phospholipids, a membrane protein might serve as an anchor for ELMO.

The change of ELMO-Sponge distribution from a disc-like to a ring-like pattern coincides with the MBT and thus might ultimately depend on one or more zygotic genes, on cell cycle regulators such as checkpoint kinases, which change their activity during MBT, or other MBT-associated processes (reviewed by Liu and Großhans, 2017). Among the early zygotic genes, the best candidate for

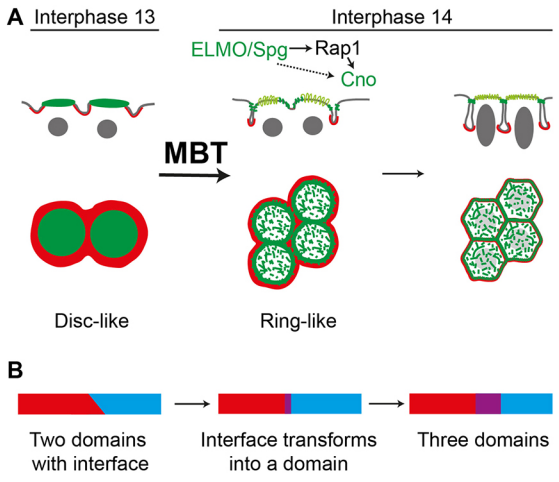

Fig. 9. Model of formation of the subapical domain. (A) Dynamics of ELMO-Sponge (green) distribution from a disc-like to ring-like pattern during the onset of interphase 14. Intercap region and basal domain are marked in red. ELMO-Sponge is a potential Rap1 activator, which in turn restricts Canoe to the subapical domain. (B) Positional information for the emergence of the subapical domain (purple) based on transformation of the domain interface.

Development (2018) 145, dev157909. doi:10.1242/dev.157909

contributing to ELMO-Sponge redistribution might be the zygotic gene *dunk*, which controls apical myosin contractility and flow at the onset of cellularization. However, a potential role of *dunk* or other zygotic genes in cortical domain formation and segregation has not been analyzed (He et al., 2016). Future experiments analyzing the detailed dynamics and factors controlling the localization of ELMO-Sponge are likely to provide insight into the underlying molecular and biophysical mechanism.

MATERIALS AND METHODS

Fly strains and genetics

Fly stocks were obtained from the Bloomington Drosophila Stock Center, unless otherwise noted. The following fly strains and mutations were used: UASp-CherrySlam driven by maternal Gal4 (Acharya et al., 2014), Df(2L)*slam* (Acharya et al., 2014), *Ced-12/ELMO*^{367} (Winkler et al., 2015), *cno*[R2] (Choi et al., 2013), CanoeYFP (*PBac{602.P.SVS-1}cno*^{CPTI000590}, Drosophila Genomics and Genetic Resources, Kyoto), *scrb-GFP*^{CA07683} (Buszczak et al., 2007), *scrb[1]* (Bilder and Perrimon, 2000), *rap1*[P5709] (R. Reuter, University of Tübingen, Germany; Knox and Brown, 2002), *sponge*[242] (Postner et al., 1992), Df(3R)3450 (deficiency uncovering *sponge*), *dizzy(Δ8)* (R. Reuter; Huelsmann et al., 2006) and GFP-Rap1 (E. Knust, Max Planck Institute, Dresden, Germany; Knox and Brown, 2002). ELMO-GFP transgenes were generated according to standard protocols by ϕC31 integrase-mediated site-specific insertions in the landing site ZH-86Fb (Bischof et al., 2007). All fly cages and crosses were maintained by standard methods at 25°C unless otherwise specified. Germline clones were induced by heat shock (each 1 h, at 24-48 h and 48-72 h of development) of first and second instar larvae and selected by ovoD transgenes on corresponding Frt chromosomes.

Molecular genetics

The genomic ELMO-GFP construct was generated by ligation of multiple fragments, which were amplified by PCR. Fragment 1-GFP (optimized for *Drosophila* codon usage), using upstream primer (5′-3′) ZL95 (tggcggccgcACTGGAAGTTCTGTTCCAGGGGCCCGGCTCCGCCGG-CTCC), introducing a *Not*I site and a PreScission cleavage site; and downstream primer ZL75 (TAAAGCTTGTACAGCTCGTCCATGCC), inserting a *Hin*dIII site. Fragment 2-ELMO3′ with a leading stop codon (chromosome 2L, 12,100543-12,101,303), using upstream primer ZL76 (ACAAGCTTTAAGCATAACGAGCACAATTAC), adding a stop codon and *Hin*dIII site; and downstream primer ZL73 (atctcgaGTCTGCCTG-CCGGACCGG), adding an *Xho*I site to the 3′ end. Both fragments were cloned (*Not*I/*Xho*I) into pBSK (Stratagene) to create BSK-GFP-ELMO3′ and transferred to the transformation vector pAttB (Bischof et al., 2007) to create pAttB-GFP-ELMO3′. Fragment 3, a 3633 bp genomic fragment encompassing the 5′ region of the *ELMO* locus to the 3′ end of *ELMO* exon 4 (chromosome 2L, 12,096,904-12,100,537). *Not*I sites were introduced on both ends by upstream primer ZL99 (AACAGATCTGCGGCCGGAAG-ACAAGCGATCGGATGC) and downstream primer ZL104 (ACTTCCAG-TgcggccgcgCTCTCAAAGCAAAAATCATAG). Fragment 3 was cloned into the *Not*I site of pAttB-GFP-ELMO3′ leading to the final transformation plasmid pAttB-ELMO-GFP-ELMO3′, which comprises DNA from the *ELMO* locus region (breakpoints are 12,096,904-12,101,303) with a PreScission cleavage site and GFP in front of the stop codon.

Immunostaining

Embryos were fixed with 4% formaldehyde or heat fixed according to standard procedures as described previously (Großhans et al., 2005) and stored in methanol. Fixed embryos were rinsed three times in PBS with 0.1% Tween 20 (PBT), and blocked in 5% bovine serum albumin (BSA) in PBT for 1 h at room temperature. Blocked embryos were incubated with primary antibodies in 0.1% BSA in PBT overnight at 4°C or at room temperature for 2 h with constant rotation. After rinsing three times and washing four times for 15 min each with PBT, the embryos were incubated with fluorescently labeled secondary antibodies in PBT for 2 h at room temperature. Following another round of rinsing and washing, embryos were stained with DAPI (0.2 µg/ml) for 10 min, rinsed three times in PBT, washed in PBT for 10 min and mounted in Aqua-Poly/Mount (Polysciences). Embryos for phalloidin staining were fixed in 8% formaldehyde and the vitelline membrane was manually removed. Primary antibodies were rabbit anti-Canoe (1:1000; Choi et al., 2013), mouse anti-Dlg (1:100, 4F3, Developmental Studies Hybridoma Bank), rabbit/guinea pig anti-Slam (1:5000; Brandt et al., 2006), guinea pig anti-Sponge (1:1000; Biersmith et al., 2011). Phalloidin coupled to Alexa Fluor 488 was obtained from Thermo Fisher. Secondary antibodies were coupled to Alexa Fluor 488, 568 and 647 (1:500, Thermo Fisher).

Western blots

Western blotting was conducted as previously described (Wenzl et al., 2010). Briefly, lysis samples corresponding to ten staged embryos (0-2 h) were separated by SDS-PAGE and transferred by wet transfer to a nitrocellulose membrane. Blots were imaged with an Odyssey CLx infrared imaging system (LI-COR Biosciences) with 16-bit depth. Primary antibodies were goat anti-ELMO (1:3000; Biersmith et al., 2011), mouse anti-α-Tubulin (1:50,000, B512, Sigma). Secondary antibodies were 800CW- or 680CW-coupled donkey anti-guinea pig/mouse/rabbit IgG (Invitrogen). Images were processed in Adobe Photoshop and Fiji/ImageJ (Schindelin et al., 2015).

Imaging

Live embryos were handled as previously described (Kanesaki et al., 2011). Fluorescent time-lapse movies and images of fixed embryos were recorded with a Zeiss LSM780 confocal microscope equipped with Airyscan detection, and objectives LCI Plan Neofluar 63×/water NA 1.3 for fixed samples, Plan Neofluar 63×/oil NA 1.4 for live imaging. Movies of embryos expressing CanoeYFP and CherrySlam were obtained with a frame size of 256×256 pixels (28.7×28.7 µm) and a lateral pixel size of 110 nm at an interval of 60 s. Channels were changed after recording of every *z*-stack; each *z*-stack had 19 slices with a step size of 0.5 µm. Embryos expressing ScribbledGFP were imaged with Airyscan detection with a frame size of 488×488 pixels (36×36 µm) and a lateral pixel size of 73 nm. Each *z*-stack included 11 slices with a step size of 1 µm, imaged at an interval of 60 s. Embryos expressing ELMO-GFP and CherrySlam were imaged with Airyscan detection with a frame size of 488×488 pixels (32×32 µm) with a lateral pixel size of 66 nm. Each *z*-stack contained 17 slices with a step size of 0.5 µm, obtained at an interval of 60 s. Images of embryos expressing GFP-Rap1 were obtained with Airyscan detection with a frame size of 476×476 pixels (32.1×32.1 µm; 67.5 nm lateral pixel size). *z*-stacks were conducted with a step size of 0.2 µm and orthogonal views were conducted with Fiji/ImageJ as well as measurement of furrow length. Fixed embryos were imaged with a frame size of 512×512 pixels (67.5×67.5 µm; 130 nm lateral pixel size) for top views and 512×200 pixels (96.4×29.4 µm; 190 nm lateral pixel size) for sagittal views. Images were processed with Fiji/ImageJ and Adobe Photoshop and Adobe Illustrator.

Image quantification

Measurements were conducted with Fiji/ImageJ, with calculation in Microsoft Excel. For the quantifications in Fig. 2E,F and Fig. 8D, fluorescence intensities were measured along three furrows in each *z* position along the apical-basal axis. The maximal intensities for each protein were normalized to 1 and plotted as a graph with apical-basal position on the *y*-axis and normalized fluorescence intensities on the *x*-axis. The heatmap in Fig. 5D was prepared by measuring the fluorescence intensity distribution along the furrows in side views in a total of nine furrows in three embryos. Intensities were normalized to 1 for every furrow and displayed as heatmaps using the conditional formatting function in Excel. Averages of normalized intensities were plotted with apical-basal position on the *y*-axis and normalized fluorescence intensities on the *x*-axis. For quantifications in Fig. 2G, the distribution of CanoeYFP fluorescence intensity at one furrow was measured in top view of live images at different time points using the line plot function of Fiji/ImageJ. Position zero on the *x*-axis was defined by the peak of the curve at the latest time point.

Acknowledgements
We are grateful to E. Geisbrecht, D. Bilder, M. Peifer, R. Reuter and E. Knust for materials or discussions. We acknowledge service support from the Developmental Studies Hybridoma Bank created by the NICHD of the NIH, USA, and maintained by the University of Iowa; the Bloomington Drosophila Stock Center (supported by NIH P40OD018537); the Drosophila Genomics and Genetic Resources, Kyoto; the BACPAC Resources Center at Children's Hospital Oakland; and the Drosophila Genomics Resource Center at Indiana University (supported by NIH 2P40OD010949-10A1).

Competing interests
The authors declare no competing or financial interests.

Author contributions
Conceptualization: Z.L., J.G.; Methodology: A.S., Z.L., J.G.; Validation: A.S., Z.L., J.G.; Formal analysis: A.S., Z.L.; Investigation: A.S., Z.L.; Resources: A.S., Z.L., J.G.; Data curation: A.S., Z.L.; Writing - original draft: A.S., J.G.; Writing - review & editing: A.S., J.G.; Visualization: J.G.; Supervision: J.G.; Project administration: J.G.; Funding acquisition: J.G.

Funding
Z.L. was in part supported by a fellowship from the China Scholarship Council. This work was in part supported by the Göttingen Centre for Molecular Biology (funds for equipment repair) and the Deutsche Forschungsgemeinschaft (Priority programme SPP1464, GR1945/4-1/2, and equipment grant INST1525/16-1 FUGG).

Supplementary information
Supplementary information available online at
http://dev.biologists.org/lookup/doi/10.1242/dev.157909.supplemental

References

Acharya, S., Laupsien, P., Wenzl, C., Yan, S. and Großhans, J. (2014). Function and dynamics of slam in furrow formation in early Drosophila embryo. *Dev. Biol.* **386**, 371-384.
Benton, R. and Johnston, D. S. (2003). Drosophila PAR-1 and 14-3-3 inhibit bazooka/PAR-3 to establish complementary cortical domains in polarized cells. *Cell* **115**, 691-704.
Biersmith, B., Liu, Z., Bauman, K. and Geisbrecht, E. R. (2011). The DOCK protein sponge binds to ELMO and functions in Drosophila embryonic CNS development. *PLoS ONE* **6**, e16120.
Biersmith, B., Wang, Z.-H. and Geisbrecht, E. R. (2015). Fine-tuning of the actin cytoskeleton and cell adhesion during Drosophila development by the unconventional guanine nucleotide exchange factors myoblast city and sponge. *Genetics* **200**, 551-567.
Bilder, D. and Perrimon, N. (2000). Localization of apical epithelial determinants by the basolateral PDZ protein Scribble. *Nature* **403**, 676-680.
Bilder, D., Schober, M. and Perrimon, N. (2003). Integrated activity of PDZ protein complexes regulates epithelial polarity. *Nat. Cell Biol.* **5**, 53-58.
Bischof, J., Maeda, R. K., Hediger, M., Karch, F. and Basler, K. (2007). An optimized transgenesis system for Drosophila using germ-line-specific phiC31 integrases. *Proc. Natl. Acad. Sci. USA* **104**, 3312-3317.
Boettner, B., Harjes, P., Ishimaru, S., Heke, M., Fan, H. Q., Qin, Y., Aelst, L. V. and Gaul, U. (2003). The AF-6 homolog canoe acts as a Rap1 effector during dorsal closure of the Drosophila embryo. *Genetics* **165**, 159-169.
Bonello, T. T., Perez-Vale, K. Z., Sumigray, K. D. and Peifer, M. (2018). Rap1 acts via multiple mechanisms to position Canoe and adherens junctions and mediate apical-basal polarity establishment. *Development* **145**, dev157941.
Brandt, A., Papagiannouli, F., Wagner, N., Wilsch-Bräuninger, M., Braun, M., Furlong, E. E., Loserth, S., Wenzl, C., Pilot, F., Vogt, N. et al. (2006). Developmental control of nuclear size and shape by kugelkern and kurzkern. *Curr. Biol.* **16**, 543-552.
Buszczak, M., Paterno, S., Lighthouse, D., Bachman, J., Planck, J., Owen, S., Skora, A. D., Nystul, T. G., Ohlstein, B., Allen, A. et al. (2007). The carnegie protein trap library: a versatile tool for Drosophila developmental studies. *Genetics* **175**, 1505-1531.
Chalmers, A. D., Pambos, M., Mason, J., Lang, S., Wylie, C. and Papalopulu, N. (2005). aPKC, Crumbs3 and Lgl2 control apicobasal polarity in early vertebrate development. *Development* **132**, 977-986.
Choi, W., Harris, N. J., Sumigray, K. D. and Peifer, M. (2013). Rap1 and Canoe/afadin are essential for establishment of apical-basal polarity in the Drosophila embryo. *Mol. Biol. Cell* **24**, 945-963.
Cohen, D., Brennwald, P. J., Rodriguez-Boulan, E. and Müsch, A. (2004). Mammalian PAR-1 determines epithelial lumen polarity by organizing the microtubule cytoskeleton. *J. Cell Biol.* **164**, 717-727.
deBakker, C. D., Haney, L. B., Kinchen, J. M., Grimsley, C., Lu, M., Klingele, D., Hsu, P.-K., Chou, B.-K., Cheng, L.-C., Blangy, A. et al. (2004). Phagocytosis of apoptotic cells is regulated by a UNC-73/TRIO-MIG-2/RhoG signaling module and armadillo repeats of CED-12/ELMO. *Curr. Biol.* **14**, 2208-2216.
Farrell, J. A. and O'Farrell, P. H. (2014). From egg to gastrula: how the cell cycle is remodeled during the Drosophila mid-blastula transition. *Annu. Rev. Genet.* **48**, 269-294.
Foe, V. E., Odell, G. M. and Edgar, B. A. (1993). Mitosis and morphogenesis in the Drosophila embryo: point and counterpoint. In *The Development of Drosophila melanogaster* (ed. M. Bate and A. Martinez Arias), pp. 149-300. Cold Spring Harbor, NY: Cold Spring Harbor Laboratory Press.
Gassama-Diagne, A. and Payrastre, B. (2009). Phosphoinositide signaling pathways: promising role as builders of epithelial cell polarity. *Int. Rev. Cell Mol. Biol.* **273**, 313-343.
Geisbrecht, E. R., Haralalka, S., Swanson, S. K., Florens, L., Washburn, M. P. and Abmayr, S. M. (2008). Drosophila ELMO/CED-12 interacts with Myoblast city to direct myoblast fusion and ommatidial organization. *Dev. Biol.* **314**, 137-149.
Großhans, J., Wenzl, C., Herz, H.-M., Bartoszewski, S., Schnorrer, F., Vogt, N., Schwarz, H. and Müller, H.-A. (2005). RhoGEF2 and the formin Dia control the formation of the furrow canal by directed actin assembly during Drosophila cellularisation. *Development* **132**, 1009-1020.
Harris, T. J. C. and Peifer, M. (2004). Adherens junction-dependent and -independent steps in the establishment of epithelial cell polarity in Drosophila. *J. Cell Biol.* **167**, 135-147.
He, B., Martin, A. and Wieschaus, E. (2016). Flow-dependent myosin recruitment during Drosophila cellularization requires zygotic dunk activity. *Development* **143**, 2417-2430.
Hermiston, M. L. and Gordon, J. I. (1995). In vivo analysis of cadherin function in the mouse intestinal epithelium: essential roles in adhesion, maintenance of differentiation, and regulation of programmed cell death. *J. Cell Biol.* **129**, 489-506.
Huelsmann, S., Hepper, C., Marchese, D., Knöll, C. and Reuter, R. (2006). The PDZ-GEF Dizzy regulates cell shape of migrating macrophages via Rap1 and integrins in the Drosophila embryo. *Development* **133**, 2915-2924.
Izumi, Y., Hirose, T., Tamai, Y., Hirai, S., Nagashima, Y., Fujimoto, T., Tabuse, Y., Kemphues, K. J. and Ohno, S. (1998). An atypical PKC directly associates and colocalizes at the epithelial tight junction with ASIP, a mammalian homologue of Caenorhabditis elegans polarity protein PAR-3. *J. Cell Biol.* **143**, 95-106.
Kanesaki, T., Edwards, C. M., Schwarz, U. S. and Grosshans, J. (2011). Dynamic ordering of nuclei in syncytial embryos: a quantitative analysis of the role of cytoskeletal networks. *Integr. Biol. (Camb)* **3**, 1112-1119.
Karr, T. L. and Alberts, B. M. (1986). Organization of the cytoskeleton in early Drosophila embryos. *J. Cell Biol.* **102**, 1494-1509.
Knox, A. L. and Brown, N. H. (2002). Rap1 GTPase regulation of adherens junction positioning and cell adhesion. *Science* **295**, 1285-1288.
Komander, D., Patel, M., Laurin, M., Fradet, N., Pelletier, A., Barford, D. and Côté, J.-F. (2008). An alpha-helical extension of the ELMO1 pleckstrin homology domain mediates direct interaction to DOCK180 and is critical in Rac signaling. *Mol. Biol. Cell* **19**, 4837-4851.
Liu, B. and Grosshans, J. (2017). Link of zygotic genome activation and cell cycle control. *Methods Mol. Biol.* **1605**, 11-30.
Martín-Belmonte, F., Yu, W., Rodríguez-Fraticelli, A. E., Ewald, A., Werb, Z., Alonso, M. A. and Mostov, K. (2008). Cell polarity dynamics controls the mechanism of lumen formation in epithelial morphogenesis. *Curr. Biol.* **18**, 507-513.
Mavrakis, M., Rikhy, R. and Lippincott-Schwartz, J. (2009). Plasma membrane polarity and compartmentalization are established before cellularization in the fly embryo. *Dev. Cell* **16**, 93-104.
McGill, M. A., McKinley, R. F. A. and Harris, T. J. C. (2009). Independent cadherin-catenin and Bazooka clusters interact to assemble adherens junctions. *J. Cell Biol.* **185**, 787-796.
Nance, J. (2014). Getting to know your neighbor: cell polarization in early embryos. *J. Cell Biol.* **206**, 823-832.
Postner, M. A., Miller, K. G. and Wieschaus, E. F. (1992). Maternal effect mutations of the sponge locus affect actin cytoskeletal rearrangements in Drosophila melanogaster embryos. *J. Cell Biol.* **119**, 1205-1218.
Raff, J. W. and Glover, D. M. (1989). Centrosomes, and not nuclei, initiate pole cell formation in Drosophila embryos. *Cell* **57**, 611-619.
Reversi, A., Loeser, E., Subramanian, D., Schultz, C. and De Renzis, S. (2014). Plasma membrane phosphoinositide balance regulates cell shape during Drosophila embryo morphogenesis. *J. Cell Biol.* **205**, 395-408.
Sawyer, J. K., Harris, N. J., Slep, K. C., Gaul, U. and Peifer, M. (2009). The Drosophila afadin homologue Canoe regulates linkage of the actin cytoskeleton to adherens junctions during apical constriction. *J. Cell Biol.* **186**, 57-73.
Schindelin, J., Rueden, C. T., Hiner, M. C. and Eliceiri, K. W. (2015). The ImageJ ecosystem: an open platform for biomedical image analysis. *Mol. Reprod. Dev.* **82**, 518-529.
Sherlekar, A. and Rikhy, R. (2017). Syndapin bridges the membrane-cytoskeleton divide during furrow extension. *Commun. Integr. Biol.* **10**, e1255832.
Spahn, P., Ott, A. and Reuter, R. (2012). The PDZ-GEF protein Dizzy regulates the establishment of adherens junctions required for ventral furrow formation in Drosophila. *J. Cell Sci.* **125**, 3801-3812.

Stephenson, R. O., Yamanaka, Y. and Rossant, J. (2010). Disorganized epithelial polarity and excess trophectoderm cell fate in preimplantation embryos lacking E-cadherin. *Development* **137**, 3383-3391.
Tanentzapf, G. and Tepass, U. (2003). Interactions between the crumbs, lethal giant larvae and bazooka pathways in epithelial polarization. *Nat. Cell Biol.* **5**, 46-52.
Wang, F., Dumstrei, K., Haag, T. and Hartenstein, V. (2004). The role of DE-cadherin during cellularization, germ layer formation and early neurogenesis in the Drosophila embryo. *Dev. Biol.* **270**, 350-363.
Warn, R. M., Bullard, B. and Magrath, R. (1980). Changes in the distribution of cortical myosin during the cellularization of the Drosophila embryo. *Development* **57**, 167-176.
Warn, R. M., Magrath, R. and Webb, S. (1984). Distribution of F-actin during cleavage of the Drosophila syncytial blastoderm. *J. Cell Biol.* **98**, 156-162.
Wenzl, C., Yan, S., Laupsien, P. and Großhans, J. (2010). Localization of RhoGEF2 during Drosophila cellularization is developmentally controlled by Slam. *Mech. Dev.* **127**, 371-384.
Winkler, F., Gummalla, M., Künneke, L., Lv, Z., Zippelius, A., Aspelmeier, T. and Großhans, J. (2015). Fluctuation analysis of centrosomes reveals a cortical function of kinesin-1. *Biophys. J.* **109**, 856-868.
Wu, Y. C. and Horvitz, H. R. (1998). C. elegans phagocytosis and cell-migration protein CED-5 is similar to human DOCK180. *Nature* **392**, 501-504.
Yajnik, V., Paulding, C., Sordella, R., McClatchey, A. I., Saito, M., Wahrer, D. C. R., Reynolds, P., Bell, D. W., Lake, R., van den Heuvel, S. et al. (2003). DOCK4, a GTPase activator, is disrupted during tumorigenesis. *Cell* **112**, 673-684.
Yuan, K., Seller, C. A., Shermoen, A. W. and O'Farrell, P. H. (2016). Timing the Drosophila mid-blastula transition: a cell cycle-centered view. *Trends Genet.* **32**, 496-507.

Supplemental data

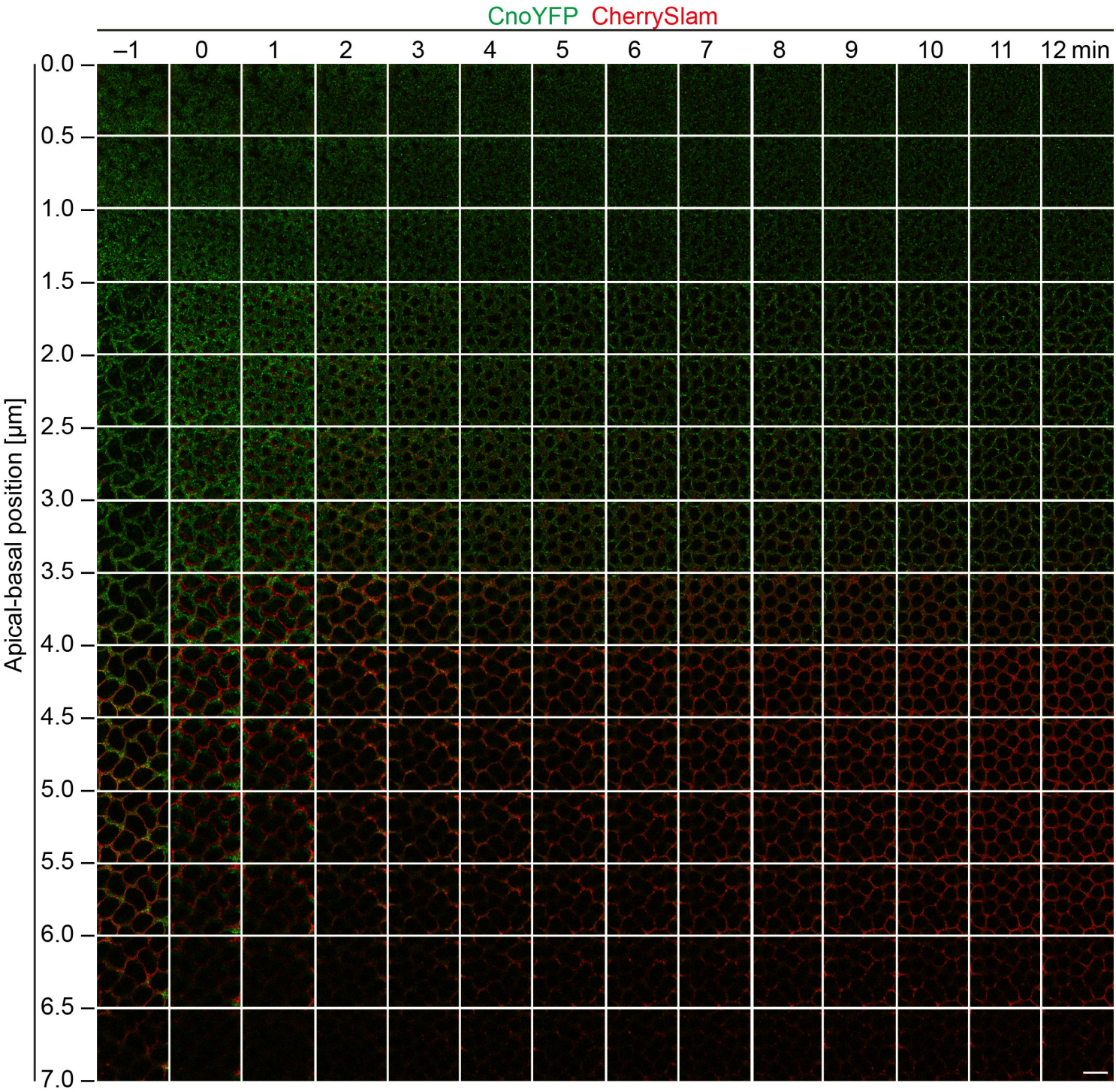

Supplemental Fig. S1. CanoeYFP and CherrySlam dynamics during mitosis 13 and interphase 14. Images from time lapse recording of an embryo expressing CanoeYFP (green) and CherrySlam (red). Time from left to right, apical basal position from up to down. Time point t=0 was defined by the emergence of a new furrow between two corresponding daughter nuclei. The spatial difference between the two color channels at t=0 and 1 min is due to a time lag in imaging as the channels were recorded one after the other. Scale bar 10 µm.

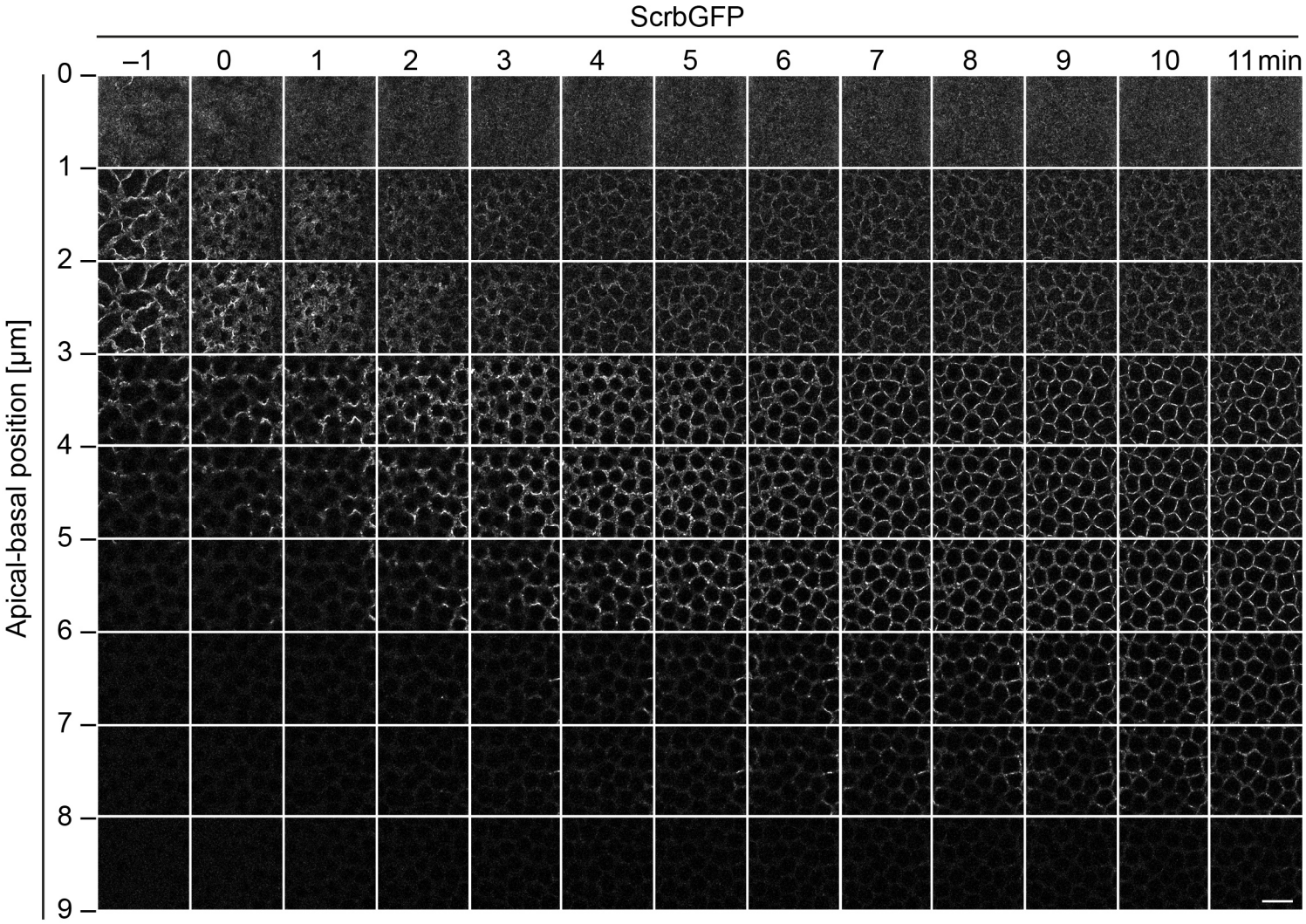

Supplemental Fig. S2. ScribbledGFP dynamics during mitosis 13 and interphase 14. Images from a time lapse recording of an embryo expressing ScribbledGFP. Time from left to right, apical basal position from up to down. Time point t=0 was defined by the emergence of a new furrow between two corresponding daughter nuclei. Scale bar 10 µm.

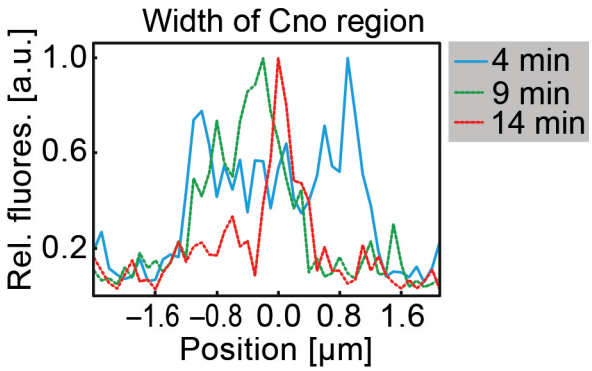

Supplemental Fig. S3. Canoe fluorescent signal narrows as the new furrow elongates. Distribution of CanoeYFP signal (relative fluorescence) across a new emerging furrow (Fig. S1) at three different time points as indicated.

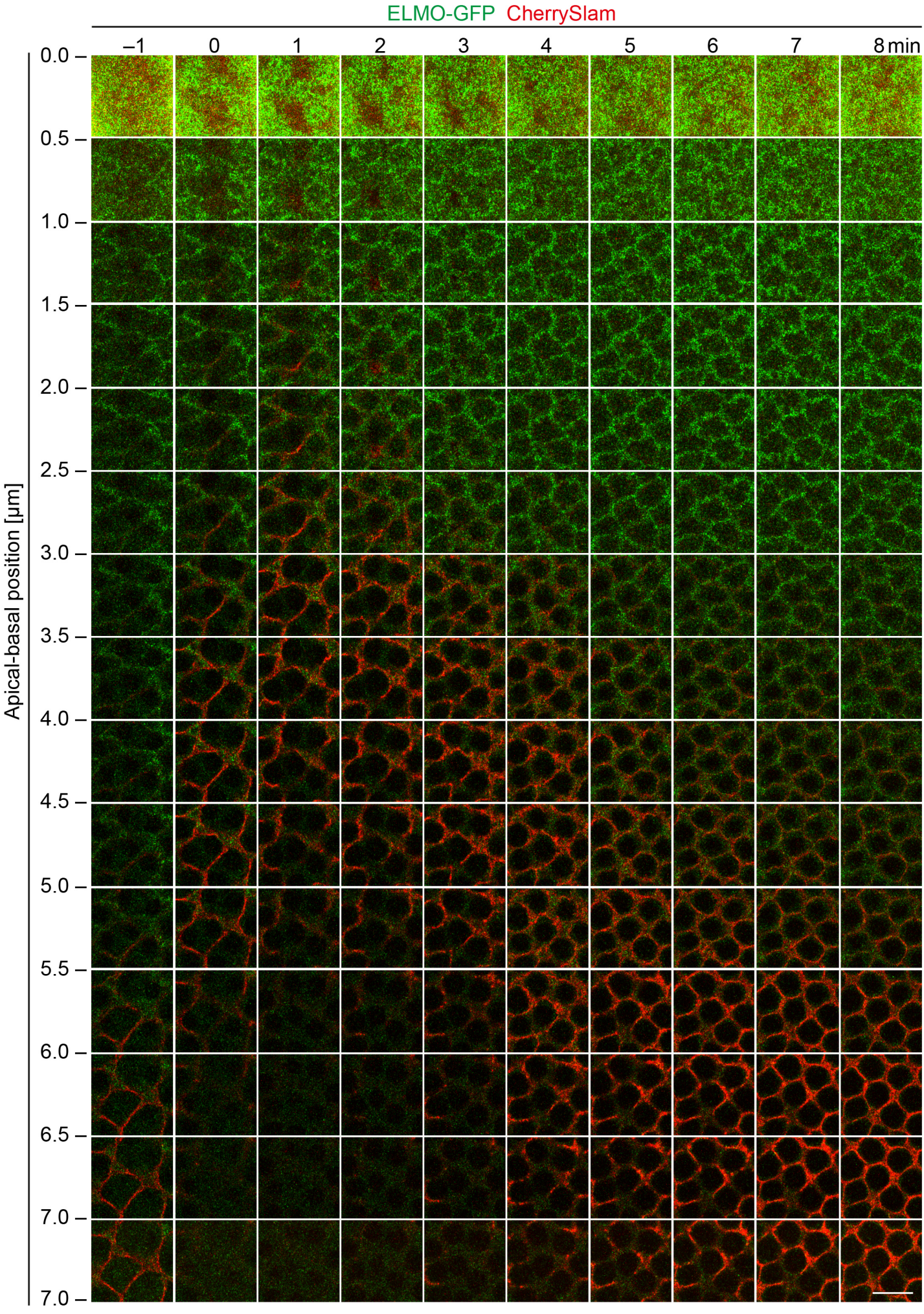

Supplemental Fig. S4. ELMO-GFP and CherrySlam dynamics during mitosis 13 and interphase 14. Images of a time lapse recording of an embryo expressing Elmo-GFP (green) and CherrySlam (red). Time from left to right, apical basal position from up to down. Time point t=0 was defined by the emergence of a new furrow between two corresponding daughter nuclei. Scale bar 10 µm.

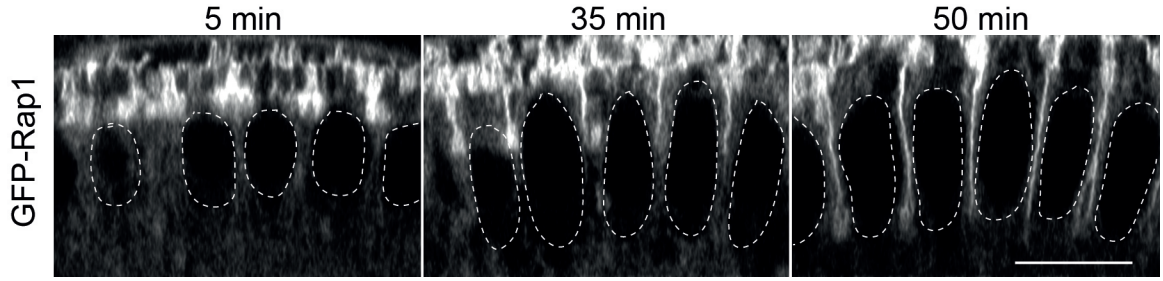

Supplemental Fig. S5. GFP-Rap1 localization during early and mid-cellularization. Images from living embryos expressing GFP-Rap1 at indicated time after onset of cellularization. Reconstructed orthogonal views from axial stacks of embryos expressing GFP-Rap1. Note that GFP-Rap1 localizes to the entire membrane without a clear enrichment at subapical, lateral or basal domain. Scale bar 10 μm.